Asian Journal of Chemistry; Vol. 28, No. 12 (2016), 2675-2679

ASIAN JOURNAL OF CHEMISTRY

http://dx.doi.org/10.14233/ajchem.2016.20068

Heating Behaviour of Iron Oxide Nanomaterials *via* Magnetic Nanoparticle Hyperthermia

C.R. LAILI* and S. HAMDAN

School of Fundamental Science, Universiti Malaysia Terengganu, 21030 K. Terengganu, Terengganu, Malaysia

*Corresponding author: Fax: +60 9 6683608; Tel: +60 1 93956167; E-mail: laili@umt.edu.my

Received: 9 May 2016; *Accepted*: 20 July 2016; *Published online*: 1 September 2016; AJC-18060

In this studies, magnetic iron oxide nanomaterial (ION) was synthesized in order to demonstrate its hyperthermia behaviour at three different frequencies. The synthesized iron oxide nanomaterial was characterized to obtain its physical properties such as surface morphology, particle size and magnetism. The iron oxide nanomaterial were subjected to hyperthermia exposed at 165.1, 173.9 and 737.5 kHz. The results obtained showed that the iron oxide nanomaterial generated good heating behaviour and were dependent on the frequencies applied with increased heating behaviour at higher frequencies.

Keywords: Nanomaterials, Iron oxide, Hyperthermia, X-ray diffraction.

INTRODUCTION

One interesting development in the use of nanomaterials is the use of magnetic nanoparticles and especially superparamagnetic iron oxide nanoparticles [1-8]. Recently, magnetic field-responsive iron oxide-loaded hollow mesoporous silica nanomaterials were synthesized using polymer nanospheres to trigger drug release on demand by magnetic hyperthermia [9]. In this work, hybrid nanomaterials provide an excellent platform for controlled drug release and hyperthermia. In another similar development, magnetoliposomes were prepared for controlled drug release to be triggered at a low frequency magnetic field [10]. A low-frequency alternating magnetic field (LF-AMF), 0.5-1000 Hz were used to study the drug release properties of unilamellar vesicles loaded with citrate coated cobalt ferrite nanoparticles. Finally, the size dependence of magnetic nanoparticles on the magnetic relaxation and specific power absorption was also reported by Lima and co-workers [11]. The experiment performed under conditions at a frequency of 250 kHz and H_0 = 13 kA/m, it was concluded that Néel/Brown relaxation is dependent on the sizes of the magnetic nanoparticle. In all the reports [9-11], the nanomaterials were exposed to magnetic fields which resulted in a quite an amount of heat being dissipated. It is known that the heating of certain organs or tissues to temperatures between 41 and 46 °C in the medical world, preferably for cancer therapy, is called hyperthermia [2].

In this work in order to understand the heating effect of iron oxide nanomaterial, magnetic nanoparticle hyperthermia (MNH) magnetic nanoparticle hyperthermia heats magnetic nanoparticles using harmless RF irradiation by magnetization reversal processes of the nanoparticles [12]. It used to heat the magnetic nanomaterials at variable frequencies. The heating pattern will be monitored.

EXPERIMENTAL

The list of chemicals used is shown in Table-1. All of the chemicals were used as received.

TABLE-1
LIST OF CHEMICALS

Experiment	Substances	Source
Synthesis of iron oxide nanomaterials	Iron(II) sulphate heptahydrate	Alfa Aesar
	Iron(III) chloride hexahydrate	Alfa Aesar
	Ammonium hydroxide	Sigma Aldrich
	Oleic acid	Sigma Aldrich
	Ethanol	Sigma Aldrich
	Hydrochloric acid	Sigma Aldrich
DLS	Toluene	Sigma Aldrich
TEM	Chloroform	Sigma Aldrich

Synthesis of iron oxide nanomaterial: A previously published method by Lopez and co-workers [13] was adopted here for the synthesis of iron oxide nanomaterial (ION) *via* co-precipitaion. Two salt solutions containing 18 g of iron(II) sulphate heptahydrate and 34 g of iron(III) chloride hexahydrate, dissolved in 175 and 200 mL of water, respectively were prepared separately. The two salt solutions were thus mixed and were then titrated with ammonium hydroxide under vigorous mechanical stirring to achieve a pH value of 10 under

inert conditions (N_2). Immediately, a small amount of oleic acid was added to the alkaline solution and the mixture stirred for 1 h at 25 °C. The resulting emulsion was heated up to 95 °C. The solution was decanted and the dark precipitate was resuspended, washed and centrifuged three times with water until the supernatant reached a pH value of 7. The precipitate was further resuspended and washed three times with ethanol. Finally, the precipitate was dried in a vacuum dessicator.

Characterization of iron oxide nanomaterial: The morphology and size of the synthesized iron oxide nanomaterial were observed using TEM, Jeol-JEM 2000EX. Its size distributions were measured using the supplied software Particle Size Analyzer (ZETA-SIZER, MALVERN Nano-ZS90) with HeNe 5 mW laser at 173°. Theiron oxide nanomaterial was analyzed for phase composition using a XRPD, Thermo ARL Xtra model (Switzerland) using Cu-K_α radiation (λ = 1.540562 Å). Finally, the magnetization data was taken using a Quantum Design MPMS SQUID VSM Magnetometer (San Diego, USA) at 300 K using a field range of ± 7 T. The samples of the synthesized iron oxide nanomaterial were dried *in vacuo* and analyzed as a solid powder.

Hyperthermia studies: Iron oxide nanomaterial in the ferrofluid was poured into the Eppendorf vial. A type T-thermocouple probe is inserted into the vial and the other end of the thermocouple terminal was attached to a computer *via* the thermocouple input of a 'MyPCLab' AD converter module. This was read using a custom-written LabView data logging routine, which displayed the data in real time and also wrote it to a DAT file for future use. This was imported to Excel for display and data processing.

The Eppendorf vial was then inserted into an insulated holder and placed directly into the sample aperture. The sample aperture was 44 mm in diameter. Care was taken to make sure the centre of the sample was located at the center of the coil (where the magnetic flux is highest). The temperature was set at 37 °C by a circulating water bath. The thermal heating effect, due to the iron oxide nanomaterials, was monitored for 600 s. The experiment was done at different frequencies.

To investigate the effect of iron oxide nanomaterial loading, samples of 0.5 mL coating containing iron oxide nanomaterials at 2, 4, 6, 8 and 10 % by weight, were filled into Eppendorfs vials. The vials are then inserted into the insulated sample holder and the resulting heating effect was monitored.

RESULTS AND DISCUSSION

Characterization of iron oxide nanomaterial: Fig. 1 shows the TEM images of the synthesized iron oxide nanomaterials. It was observed that iron oxide nanomaterials prepared using this method showed slight non-uniformity in terms of shape and size and is therefore polydisperse. DLS was employed as an additional method to determine the particle size and distribution. This size is then compared with that of equivalent data but from the TEM measurement as shown in Table-2.

TABLE-2
MEAN DIAMETER FROM TEM AND DLS MEASUREMENT. FOR TEM, THE PARTICLES WERE MEASURED FROM THE MICROGRAPHS IN ORDER TO ELUCIDATE MEAN AND STANDARD DEVIATION (SD). PDI = POLYDISPERSITY INDEX

Mean diameter ± S.D., nm		
TEM	DLS	PDI
8.7 ± 3.8	20.4 ± 1.5	0.39

From the result, the hydrodynamic diameter measured by DLS was found to be larger than the size determined from TEM. This is expected since the hydrodynamic diameter includes the oleic acid stabilizing ligand layer and the iron oxide nanoparticle core. For convenience, the mean diameter of iron oxide nanomaterials obtained by DLS in Table-2 is rounded to 20 nm from this point onward, when discussing the properties and behaviour of the particles.

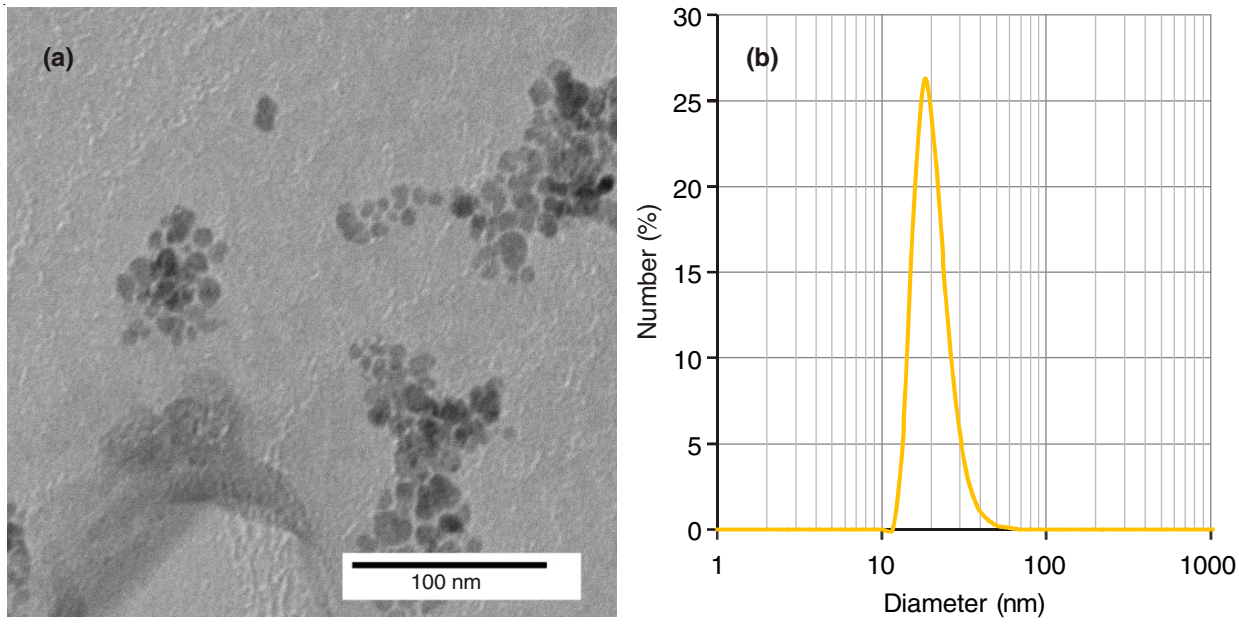

Fig. 1. (a) TEM images showing the iron oxide nanomaterials prepared by co-precipitation method with 4 mL of oleic acid and (b) the particle size distribution by DLS of iron oxide nanoparticles described as number, percent (%) synthesized

Fig. 2 shows X-ray diffraction (XRD) patterns of the iron oxide nanomaterial. It was observed that a series of peaks occurred at different 2θ values. The XRD peaks observed were at 2θ = 30.13, 35.41, 43.04, 57.07 and 62.86°. These peaks correspond to (220), (311), (400), (422) and (440) Bragg reflections, respectively. Similar peaks were observed by previously published reports indicating a cubic crystal system [14,15].

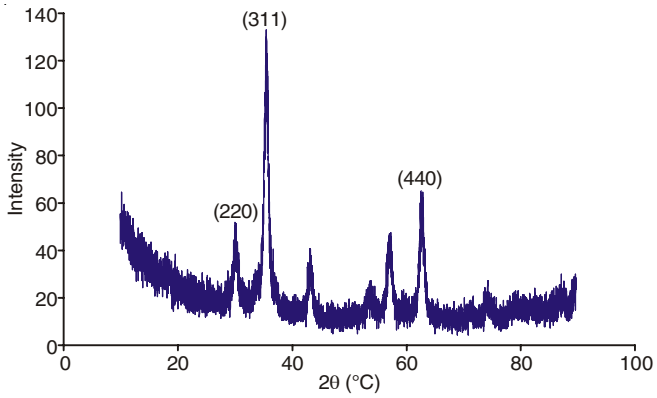

Fig. 2. XRD pattern of iron oxide nanomaterials

Among these peaks, it was observed that three strong peaks stood out, the strongest one being the (311) Bragg reflection at 2θ = 35.41° followed by (440) and (220). The parameters for all of the three strong XRD peaks at (220), (311) and (440) were calculated for their d-spacing values and intensity ratio, I/I_1. These values were then tabulated and compared with those of standard iron oxide as presented in the JCPDS Card Number 19-629, 4-755 and 13-534 for standard magnetite, γ-maghemite and hematite, respectively as shown in Table-3.

From the table, the type of iron oxide nanoparticle can be inferred. This can be achieved by comparing each of the d-spacings for every particle size at different Bragg reflection angles with the standard data. For instance, the d-spacings at (220), (311) and (440) peaks give a value of 2.964, 2.522 and 1.479 Å, respectively. These values, when compared to the standard data, closely matched that of the corresponding standard cubic phase of magnetite of 2.97, 2.53 and 1.49 Å (Table-3). This illustrated that the XRD pattern for the iron oxide nanoparticle with particle size 20 nm is that of magnetite. However, it is worth noting here that for the particle size of 20 nm, the pattern may also resemble that of γ-maghemite. This might be reasonable since magnetite easily converts to γ-maghemite upon oxidation. However, since the value for the size of the particles is incredibly small and that it is near not possible to state with conviction whether it is magnetite or γ-maghemite. It is clear that the samples do not resemble that of standard hematite, since the hematite XRD pattern has no peaks at (311) and (440) (Table-3).

The magnetization property of the synthesized iron oxide nanomaterials was studied using a superconducting quantum interference device (SQUID) magnetometer (Fig. 3). The curve increased sharply from the origin and then reduces its slope until it reaches a plateau representing the saturation magnetization. It is observed that the value for the saturation magnetization (Ms) is 77 emu/g when the applied field reaches 2000 (oe) and the coercivity (Hc) approximately is zero Oersteds (oe). The zero coercivity is indicative of the iron oxide nanomaterial becomes superparamagnet and exhibit superparamagnetism behaviour of the iron oxide nanomaterial. The resulting iron oxide nanomaterial also responded well to an external magnet as shown in the inset of Fig. 3. This ability gives it the unique advantage in working in biological environments *i.e.* applying magnetic field only when needed and at an appropriate time or interval.

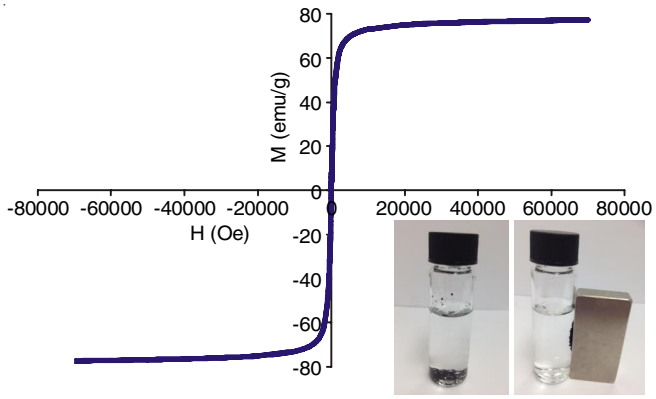

Fig. 3. Magnetic hysteresis of iron oxide nanomaterial measured using a Quantum Design MPMS SQUID VSM Magnetometer (San Diego, USA) at 300 K using a field range of ± 70000 Oe (± 7T). Inset is the photograph of iron oxide nanomaterial and its response to an external magnet

Hyperthermia studies: The characterized iron oxide nanomaterial of size 20 nm was used in order to observe its heating ability. Various frequencies of RF radiation produced by an external RF device (magneTherm) using various coils turn were applied in order to observe the heating effect. When a magnetic field at various frequencies is applied, the iron oxide nanomaterials, being superparamagnetic, will gain magnetism and start to oscillate. This oscillation will then generate heat during exposure to the magnetic field. The heating temperature was then measured and plotted. The values for the frequencies, voltage, current and magnetic field are shown in Table-4.These

TABLE-3
XRD EXPERIMENTAL DATA AT DIFFERENT PARTICLE SIZES AND COMPARING THEM WITH THE STANDARD IRON OXIDE DATA FROM JCPDS CARD

Lattice (hkl)	2θ (°)	$I/I_{1,\,expt}$	d_{expt} (Å)	JCPDS Card Number					
				19-629 magnetite		4-755 γ-maghemite		13-534 hematite	
				I/I_1	d (Å)	I/I_1	d (Å)	I/I_1	d (Å)
(220)	30.13	34.61	2.964	30	2.97	34	2.95	8	1.26
(311)	35.41	100.00	2.522	100	2.53	100	2.52	–	No peak
(440)	62.86	52.66	1.479	40	1.49	53	1.48	–	No peak

TABLE-4
VALUES OF FREQUENCIES, VOLTAGE, CURRENT AND MAGNETIC FIELD (www.nanotherics.com)

Nominal frequency (kHz)	DC power supply voltage (V)	DC power supply current (A)	Magnetic field (mT)
109.9	26.5	12.4	25.0
173.9	14.6	12.2	23.0
737.5	17.3	7.3	17.0

values are also within the accepted literature values for successful hyperthermia and are reported to be safe for humans in the range 0.1-1 MHz [16].

As a way of illustration on the heating behaviour, Fig. 4 showed the time-dependent temperature curves for iron oxide nanomaterial at 737.5 kHz. It was observed that the figure showed a non-linear relationship. Heating rates are higher initially, but progressively slows down and eventually the temperature equilibrates. Presumably this is the temperature at which heat loss to the environment is equal to heat input from the hyperthermia heating effect. Similar behaviour was observed for other frequencies.

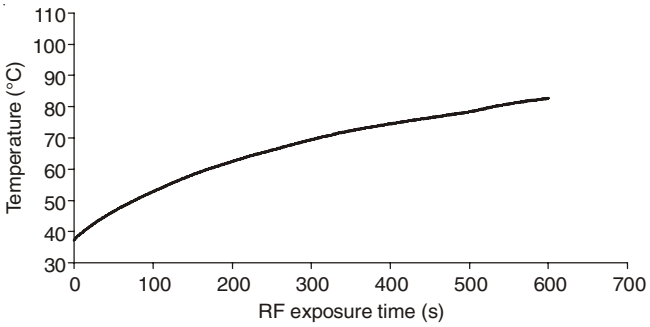

Fig. 4. Heating curve exposed at 737.5 kHz

Fig. 5 summarized the results obtained from the heating curves at variable frequencies where the maximum temperatures are plotted against their corresponding frequencies after 600 s exposure time. With the information available from the figure, the heating behaviour became more obvious. A direct relationship was observed for the maximum heating temperatures with the frequencies. It was observed that after being exposed for 600 s, the maximum temperature ranged from 55.3 to 82.8 °C. The maximum temperature reached 82.8 °C for the iron oxide nanomaterial exposed at 737.5 Hz.

The variation in the heating rate of temperature observed at different frequencies (Fig. 5) may be explained by their dependency on the spin relaxation processes. This phenomenon has been predicted by Rosensweig [17] for iron oxide nanomaterial. In general, heating occurs due to hysteresis losses and spin relaxation. Since in this case the iron oxide nanomaterial used are superparamagnetic, heating cannot occur due to the hysteresis losses since they show negligible hysteresis, therefore the observed heating must be due to the spin relaxation processes namely Néel and/or Brown relaxation. Overall, the net heating depends on which relaxation dominates. For high heating effect, it has been demonstrated elsewhere that the Brown relaxation must dominate the Néel relaxation [17]. It has also been demonstrated that the Brown relaxation

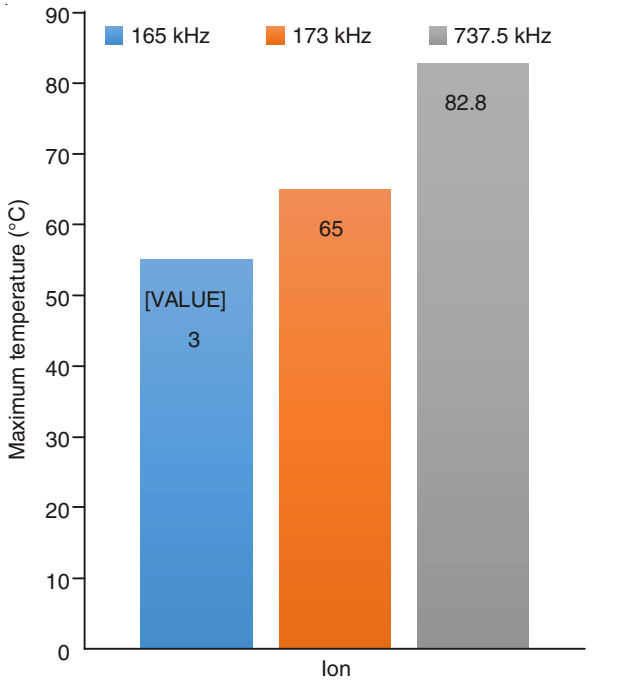

Fig. 5. Variation of maximum heating temperatures at different frequencies after 600 s exposure

becomes more effective as the particle size is increased [17]. It is worth noting here that the cross over from Néel to Brown and *vice versa* does not only depend on the frequencies but is also dependent on many other variables such as the particle size, saturation magnetization, Ms, magnetic anisotropy and applied magnetic field. In the context of size, theory shows that there exists a critical value where both relaxations contribute equally. Above that critical size, Brown relaxation dominates [18].

Conclusion

It is concluded that iron oxide nanomaterial generated good heating behaviour and are dependent on the frequencies applied. However, at this juncture it is speculated that the increase of the heating temperature with the increment of frequencies is due to the dominance of the Brown relaxation. More work needs to be done to investigate the effect of various other variables before any conclusive remark can be made. This is however, left as a subject for future work.

ACKNOWLEDGEMENTS

This work is supported by Fundamental Research Grant from Ministry of Higher Education, Malaysia (Grant No. 59364) and is gratefully acknowledged.

REFERENCES

1. J.M.D. Coey, Magnetism and Magnetic Materials, p. 1 (2010).
2. A. Jordan, R. Scholz, P. Wust, H. Fähling and R. Felix, *J. Magn. Magn. Mater.*, **201**, 413 (1999).
3. C.B. Murray, C.R. Kagan and M.G. Bawendi, *Annu. Rev. Mater. Sci.*, **30**, 545 (2000).
4. L. Mazzola, *Nat. Biotechnol.*, **21**, 1137 (2003).
5. R. Paull, J. Wolfe, P. Hebert and M. Sinkula, *Nat. Biotechnol.*, **21**, 1144 (2003).
6. Q.A. Pankhurst, J. Connolly, S.K. Jones and J. Dobson, *J. Phys. D Appl. Phys.*, **36**, R167 (2003).
7. S. Lecommandoux, O. Sandre, F. Checot and R. Perzynski, *Prog. Solid State Chem.*, **34**, 171 (2006).

8. S.R. Bhattarai, R.B. Kc, S.Y. Kim, M. Sharma, M.S. Khil, P.H. Hwang, G.H. Chung and H.Y. Kim, *J. Nanobiol.*, **6**, 1 (2008).
9. F. Lu, A. Popa, S. Zhou, J.J. Zhu and A.C.S. Samia, *Chem. Commun.*, **49**, 11436 (2013).
10. S. Nappini, M. Bonini, F.B. Bombelli, F. Pineider, C. Sangregorio, P. Baglioni and B. Norden, *Soft Matter*, **7**, 1025 (2011).
11. E. Lima, T.E. Torres, L.M. Rossi, H.R. Rechenberg, T.S. Berquo, A. Ibarra, C. Marquina, M.R. Ibarra and G.F. Goya, *J. Nanopart. Res.*, **15**, 1654 (2013).
12. R. Hergt, S. Dutz, R. Müller and M. Zeisberger, *J. Phys. Condens. Matter*, **18**, S2919 (2006).
13. M.T. López-López, J.D.G. Durán, A.V. Delgado and F. González-Caballero, *J. Colloid Interf. Sci.*, **291**, 144 (2005).
14. W. Voit, D.K. Kim, W. Zapka, M. Muhammed and K.V. Rao, *Mater. Res. Soc.*, **676**, 781 (2001).
15. F.O. Cedeno, M.M. Prieto, A. Espina and J.R. Garcia, *Thermochim. Acta*, **369**, 39 (2001).
16. T. Atsumi, B. Jeyadevan, Y. Sato and K. Tohji, *J. Magn. Magn. Mater.*, **310**, 2841 (2007).
17. R.E. Rosensweig, *J. Magn. Magn. Mater.*, **252**, 370 (2002).
18. P.D. Pino and B. Pelaz, in eds: J.M. de la Fuente and V. Grazu, Hyperthermia Using Inorganic Nanoparticles, In: Nanobiotechnology: Inorganic Nanoparticles vs. Organic Nanoparticles, Elsevier, Amsterdam, vol. 4, Chap. 13, pp. 309-319, (2012).